

Volatilization and Transport Mechanisms During Cr Oxidation at 300 °C Studied In Situ by ToF-SIMS

Clément Poulain¹ · Antoine Seyeux¹ ·
Svetlana Voyshnis¹ · Philippe Marcus¹

Received: 10 February 2017 / Published online: 28 February 2017
© Springer Science+Business Media New York 2017

Abstract The oxidation of chromium at 300 °C was investigated in situ by ToF-SIMS for three different oxygen pressures ($P_{\text{O}_2} = 2.0 \times 10^{-7}$, 6.0×10^{-7} and 2.0×10^{-6} mbar). Sequential exposure to the ^{18}O isotopic tracer was performed to reveal the governing transport mechanism in the oxide film. The evolution of the oxide thickness was monitored. Volatilization of Cr_2O_3 was evidenced. A model was used to describe the kinetics resulting from the measurements. Both the parabolic and volatilization constants showed a dependence on oxygen partial pressure like $P_{\text{O}_2}^{-1/n}$, with $n = 1.9 \pm 0.1$, indicating a defect structure mainly consisting of oxygen vacancies. The re-oxidation in $^{18}\text{O}_2$ shows a growth of the oxide layer at the metal/oxide interface, demonstrating an oxidation process governed by anionic transport via oxygen vacancies. The diffusion coefficient of oxygen in the oxide was determined by fitting the ToF-SIMS depth profiles. It is $2.0 \times 10^{-18} \text{ cm}^2 \text{ s}^{-1}$.

Keywords ToF-SIMS · In situ oxidation · Transport mechanism · Chromium

✉ Philippe Marcus
philippe.marcus@chimie-paristech.fr
Clément Poulain
clement.poulain@chimie-paristech.fr
Antoine Seyeux
antoine.seyeux@chimie-paristech.fr
Svetlana Voyshnis
svetlana.voyshnis@chimie-paristech.fr

¹ Institut de Recherche de Chimie Paris/Physical Chemistry of Surfaces Group, CNRS – Chimie ParisTech, 11 rue Pierre et Marie Curie, 75005 Paris, France

Introduction

Understanding the early stage oxidation of metals and alloys is important for several materials applications in oxidizing environments. With stainless steels now favored over ceramics as interconnects in solid oxide fuel cells (SOFC) operating at 850 °C, Cr evaporation from the oxide/gas interface has become a critical issue [1]. Significant performance degradation is encountered when the evaporated species, namely CrO₃ and CrO₂(OH)₂, deposit and poison the cathode [2]. A similar issue exists in the incineration waste industry in a chlorine environment or in combustion [3, 4], and in the nuclear industry with the use of lead–bismuth eutectic (LBE) as nuclear coolant [5]. The loss of Cr from stainless steels and Ni-base alloys is also a serious problem in gas turbines, for operating conditions at 600 °C [6].

On alloys containing Cr, involved in most applications described above, and in many other applications, a protective Cr₂O₃ layer is formed on the surface and provides a good compromise between corrosion resistance and physical properties when exposed to oxygen [1, 7–13]. The growth and transport mechanisms at stakes in chromia are hence of major technological interest, and at present the cationic or anionic nature of diffusion remains unclear, as well as the nature of defects [14]. Cr₂O₃ developed on pure chromium has been described as *p*- or *n*-type semiconductor depending on the oxygen partial pressure [15–17]. At high *P*_{O₂} pressure, Cr₂O₃ is a *p*-type semiconductor with electron holes and chromium vacancies as the predominant defects; at intermediate *P*_{O₂}, Cr₂O₃ behaves as an intrinsic semiconductor with electrons and electron holes as the major defects; at low *P*_{O₂}, Cr₂O₃ changes to an *n*-type semiconductor with electrons and chromium interstitials as the dominant defects. It is also mostly this layer that is altered due to volatilization at high temperature, leading to performance degradation.

The common aspect of these different applications in which volatilization occurs is that they are high temperature applications. Here, we will report on the volatilization from a pure Cr sample exposed to O₂ at 300 °C in an ultra-high vacuum (UHV) environment, temperature at which, to the best of our knowledge, it has never been reported. The evolution of the oxide film thickness was followed in situ by time of flight secondary ion mass spectrometry (ToF-SIMS) for three oxygen partial pressures, which allowed us to determine the nature of defects in the Cr₂O₃ layer. The nature of diffusion in the oxide film was evidenced by a two-stage oxidation experiment using ¹⁶O and ¹⁸O as tracer, and fitting the ToF-SIMS depth profiles allowed us to determine the diffusion coefficient.

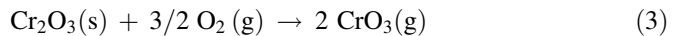
Models by Wagner [18], and Cabrera and Mott [19], were the original models for the growth kinetics of an oxide film, based on ionic transport. The diffusion of ions in Wagner's model takes place at high temperature. Migration occurs by jumping from normal lattice sites to adjacent vacant sites or some other point defect. The rate of oxide growth takes thus the form:

$$\frac{dx}{dt} = \frac{k_p}{x}, \quad \text{and} \quad x^2 = 2k_p t \quad (1, 2)$$

where *k_p* is the parabolic constant.

The Cabrera–Mott (CM) model considers a dissociative adsorption of oxygen molecules on the oxide surface, giving rise to electron traps and a potential drop V across the film [19]. This drop allows a decrease of the activation energy W for the movement of ions according to: $W - 1/2(qaF)$, q being the charge on the ion, a the jump distance and $F = V/x$ the electrical field, x being the thickness of the oxide film. This approach and its modifications lead to logarithmic and inverse logarithmic laws [20, 21].

Tedmon first established a model that takes into account the surface reaction leading to volatilization of Cr_2O_3 on a pure Cr sample at 1000 °C during the exposition to oxygen according to the following equation [22]:



This model is in principle applicable at any temperature provided that volatilization occurs at this temperature. According to Sabioni et al. [14], the higher the temperature and the oxygen partial pressure are, the more important this evaporation phenomenon is. Although it is assumed that evaporation occurs at temperatures above 700 °C, it has not been demonstrated that this phenomenon does not occur at lower temperature. The growth rate which takes into consideration this phenomenon is a modification of Wagner's approach by adding a constant of volatilization k_v that slows down the apparent kinetics in the following way:

$$\frac{dx}{dt} = \frac{k_p}{x} - k_v \quad (4)$$

which gives after integration:

$$t = \frac{k_p}{k_v^2} \left[-\frac{k_v}{k_p} x - \ln \left(1 - \frac{k_v}{k_p} x \right) \right] \quad (5)$$

Experimental Procedures

Measurements were taken using a dual-beam ToF-SIMS V spectrometer (ION-TOF GmbH, Muenster, Germany). The base pressure in the analysis chamber is maintained at $<5.0 \times 10^{-9}$ mbar in normal operating conditions. In order to describe the oxidation kinetics of Cr, starting from a clean and metallic surface, a preparation method was elaborated. After mechanical polishing up to $1/4 \mu\text{m}$ (using diamond paste), the sample was introduced in the analysis chamber and the sputtering ion gun was used to perform a first Ar^+ sputtering over an area of 1mm^2 at 2 keV in order to clean the surface. In order to degas the different components in the chamber, an annealing at 400 °C during 1 h was applied, followed by another sputtering. The Ar^+ ion gun was then switched off, and the sample was maintained at a temperature of 300 °C during 1 h in order to pump the remaining Ar gas in the chamber and lower the pressure until it was below 1.0×10^{-8} mbar. A clean chromium surface was obtained with this surface preparation procedure. Oxidation was performed by O_2 introduction in the analysis chamber through a precision

valve. The three oxygen partial pressures for which kinetics were performed are 2.0×10^{-7} , 6.0×10^{-7} and 2.0×10^{-6} mbar.

A Bi^+ primary ion source that scanned over an area of $30 \times 30 \mu\text{m}^2$ was used as the analysis beam, with a 1.2 pA current for the $P_{\text{O}_2} = 2.0 \times 10^{-7}$ mbar and $P_{\text{O}_2} = 2.0 \times 10^{-6}$ mbar experiments. ToF-SIMS depth profiles were measured with the instrument working in the dual-beam mode, and the sputtering was performed using a 20 nA (1 keV) Cs^+ ion beam for the $P_{\text{O}_2} = 2.0 \times 10^{-7}$ mbar kinetics. Cs^+ beam current was 25 nA for the $P_{\text{O}_2} = 2.0 \times 10^{-6}$ mbar kinetics. The beam sputtered an area of $100 \times 100 \mu\text{m}^2$ in both cases. Since the technique used is destructive, each measurement was taken at a different location in the 1mm^2 surface that was cleaned on the sample at the beginning of the experiment.

In order to have access to the growth mechanism of the chromia oxide film, the oxidation performed at $P_{\text{O}_2} = 6.0 \times 10^{-7}$ mbar was then followed by an in situ re-oxidation in isotopic $^{18}\text{O}_2$ gas. The first ^{16}O stage oxidation occurred for 210 min before the oxygen valve on analysis chamber was closed. The sample was then maintained at 200 °C, while $^{16}\text{O}_2$ was pumped out of the line and replaced with the $^{18}\text{O}_2$ isotopic tracer. The second stage experiment was then performed at the same pressure and temperature (6.0×10^{-7} mbar, 300 °C and during 210 min). The Bi^+ and Cs^+ beam currents were settled at 0.1 pA and 7 nA (500 eV), respectively, due to saturation of ^{18}O signal for higher values.

Results and Discussion

Depth on ToF-SIMS profiles is usually expressed as the sputtering time. The depth of the craters produced during ToF-SIMS analysis was measured by mechanical profilometry providing an independent measurement of the thickness of the depth profile. The measured sputtering rates were 0.7, 0.1 and 0.8nm s^{-1} for $P_{\text{O}_2} = 2.0 \times 10^{-7}$ mbar, $P_{\text{O}_2} = 6.0 \times 10^{-7}$ mbar and $P_{\text{O}_2} = 2.0 \times 10^{-6}$ mbar kinetics, respectively (note that sputtering conditions are function of the oxygen pressure). The sputtering rates were assumed constant during the study of the evolution of the oxide thickness and were used to plot the depth profile in nm scales.

In his crossed X ray diffraction (XRD) and ToF-SIMS study of Cr oxidation, Mazenc et al. [23, 24] showed that CrO^- and CrO_2^- signals are characteristics of Cr_2O_3 , in ToF-SIMS profiles. A very small amount of oxide was formed due to the degassing of components in the analysis chamber at 300 °C. The surface was considered clean enough to start the oxidation study.

Figure 1 shows the evolution with exposure time of the oxide thickness during oxidation at 300 °C for the three different O_2 pressures. A first observation is the dependence on oxygen pressure of the kinetics. While it remains difficult to discriminate between the oxidation rates for $P_{\text{O}_2} = 6.0 \times 10^{-7}$ mbar and $P_{\text{O}_2} = 2.0 \times 10^{-6}$ mbar for short exposure times, the lowest pressure one, for $P_{\text{O}_2} = 2.0 \times 10^{-7}$ mbar, appears to be higher. Another important feature emphasized by Fig. 1 is the way the maximum thickness reached by the oxide layer during the kinetics evolves with the oxygen pressure. Exposure to the intermediate measured

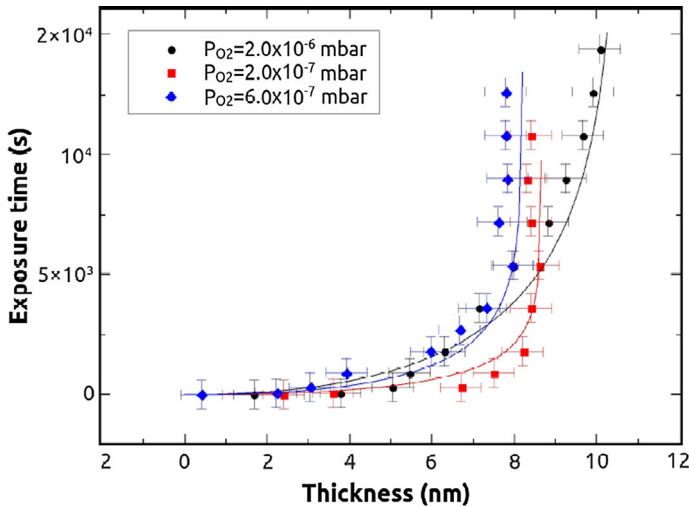


Fig. 1 Oxidation kinetics of Cr for three oxygen pressures. Fit of the kinetics by Eq. 5 (solid lines)

pressure ($P_{O_2} = 6.0 \times 10^{-7}$ mbar) results indeed for long times in the formation of the thinnest oxide layer, whereas lowest and highest pressures form the intermediate and thickest layers, respectively. This behavior, as will be seen further on, is the result of a competition between parabolic growth and volatilization in the oxide layers, as well as their dependence on P_{O_2} .

The three kinetics of Fig. 1 are fitted with Eq. (5) (Tedmon model) for Cr_2O_3 volatilization. The Tedmon model has been used since direct evidence of volatilization of Cr_2O_3 has been obtained during this in situ oxidation experiment, looking at the Cr deposition on a Si surface, maintained at room temperature, located close to the FeCr sample oxidized at low oxygen pressure, at 300 °C. The parabolic constant, k_p , of the Wagner and Tedmon models is a function of the diffusion coefficients of the oxidation governing species [18]. The volatilization constant of Tedmon, k_v , is linked to Eq. (3) and the amount of oxygen reacting with Cr_2O_3 on the surface [14, 22]. The values of the k_p and k_v constants for the three pressures are reported in Table 1.

The data in Table 1 show a decrease of the constants with increasing oxygen pressure and evolve like $P_{O_2}^{-1/2}$. For example, let us consider the first two lowest

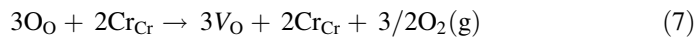
Table 1 Parabolic and volatilization constants of the Tedmon model (Eq. 5) for the three kinetics of Fig. 2

P_{O_2} (mbar)	k_p (nm ² s ⁻¹)	k_v (nm s ⁻¹)
2.0×10^{-7}	$5.8 \pm 0.1 \times 10^{-2}$	$6.7 \pm 0.1 \times 10^{-3}$
6.0×10^{-7}	$3.2 \pm 0.1 \times 10^{-2}$	$3.9 \pm 0.1 \times 10^{-3}$
2.0×10^{-6}	$1.9 \pm 0.1 \times 10^{-2}$	$1.8 \pm 0.1 \times 10^{-3}$

oxygen pressures, $P_{O_2} = 2.0 \times 10^{-7}$ mbar and $P_{O_2} = 6.0 \times 10^{-7}$ mbar. Those will be noted P^1 and P^2 , respectively. The k_{p1}/k_{p2} ratio gives an approximate value of 1.8 ± 0.1 , in good agreement with $(P^1/P^2)^{-1/2}$, which is equal to 1.7 ± 0.1 . The same goes with k_{v1}/k_{v2} which is also equal to 1.7 ± 0.1 . The measured oxidation dependence on pressure, as described by the Tedmon model [Eq. (5)] in Fig. 1, can thus be expressed as:

$$k_p \propto P_{O_2}^{-1/2} \ \& \ k_v \propto P_{O_2}^{-1/2} \quad (6)$$

Let us now focus on the nature of defects in the oxide layer since the diffusion coefficient is generally assumed to be directly proportional to their concentration [18, 25]. Equation (7) describes the formation of oxygen vacancies, V_O :



O_O et Cr_{Cr} indicate oxygen and chromium ions on their normal lattice sites, respectively. The equilibrium constant for (7) is expressed as:

$$K = (V_O)^3 \cdot P_{O_2}^{3/2} \quad (8)$$

with the brackets indicating the concentration. This gives for the defects concentration:

$$V_O \propto P_{O_2}^{-1/2} \quad (9)$$

Assuming a defect structure mostly consisting of oxygen vacancies in Cr_2O_3 implies then that their concentration in the oxide layer is proportional to $P_{O_2}^{-1/2}$. As it was mentioned earlier, the parabolic constant, k_p , is expressed as a function of the diffusion coefficient of the oxidation governing species. Although major discrepancies were reported on the relative diffusion coefficients for oxygen and chromium, recent studies attributed a higher diffusivity to oxygen ions in chromia [14, 26, 27]. We will thus consider k_p to be expressed, as previously demonstrated by Wagner [18], as:

$$k_p = \int_{P_{O_2}^1}^{P_{O_2}} D_O d \ln P_{O_2} \quad (10)$$

where $P_{O_2}^1$ is the oxygen partial pressure at the metal/oxide interface and D_O is the diffusion coefficient of the oxygen ions. The diffusion coefficient being proportional to the defects concentration, it is also proportional to $P_{O_2}^{-1/2}$ (Eq. 9), and we will therefore have a parabolic constant proportional to $P_{O_2}^{-1/2}$ after integration. This dependence on oxygen pressure implies that, for our operating pressures and temperature, the Cr_2O_3 growth on Cr is governed by inward oxygen diffusion through oxygen vacancies in the oxide layer. We will see, further on, that this interpretation was confirmed by the two-stage oxidation experiment using ^{18}O as isotopic tracer.

The volatilization constant, k_v , follows the same dependence on oxygen pressure than k_p (Eq. 6). This can be understood by the preferential dissociative adsorption sites of O_2 . These sites are assumed to be defects on a growing Cr_2O_3 layer surface [28]. The amount of oxygen that reacts with Cr_2O_3 to give $CrO_3(g)$ (Eq. 3) (reaction that is at the origin of volatilization at the oxide/ $O_2(g)$ interface) is thus proportional to the amount (V_O) of defects. The volatilization constant, proportional to the amount of reactive oxygen, is therefore proportional to $P_{O_2}^{-1/2}$ like k_p . It appears then that the mechanisms of both reactions taking place during the oxidation of chromium for our operating oxygen pressures and temperature are closely related to the defects structure in the oxide layer.

Let us now consider at which interface a new oxide forms after a first oxidation of chromium. To do so, an exposure to the ^{18}O isotopic tracer was performed after the sample was exposed to $^{16}O_2$ during 210 min at 300 °C ($P_{O_2} = 6.0 \times 10^{-7}$ mbar, blue curve on Fig. 1). This two-stage oxidation experiment could bring confirmation on the nature of diffusion and defects structure that we deduced from the oxidation kinetics experiments (Fig. 1). An anionic diffusion, i.e. inward oxygen diffusion, would indeed mean an ^{18}O oxide formation at the metal/oxide interface, whereas a cationic diffusion, i.e. outward Cr diffusion, would imply a formation at the oxide/ $O_2(g)$ interface.

Figure 2a shows the percentage of $^{16}O^-$ and $^{18}O^-$ in the oxide as function of depth measured during the exposure of the chromium sample to $^{18}O_2$. As mentioned in the experimental section, the sample was first oxidized with an exposure to $^{16}O_2$ during 210 min and then to $^{18}O_2$ during 1 min. What appears clear on Fig. 2a is that the new oxide forms at the metal/oxide interface, indicating that the oxide grows by anionic diffusion. A similar conclusion (oxide growth at the metal/oxide interface) can also be done from the ToF-SIMS depth profile obtained after 155 min of re-oxidation in $^{18}O_2$ (Fig. 2b). The two-stage oxidation experiment confirms then that oxygen is the growth governing species and that it diffuses through the oxide layer to react with cations at the metal/oxide interface. Although the latter experiment does not allow to discriminate between short circuits (grain boundaries) and lattice diffusion, our study of the parabolic constant, k_p , and the oxidation kinetics shows that oxygen ions diffuse through oxygen vacancies in the oxide layer. Among our results, the inward growth of Cr_2O_3 is in agreement with prior publications on oxidation performed at higher temperature [14, 26, 27] that show that oxygen diffusion in Cr_2O_3 is faster than chromium diffusion.

Beyond the oxide/metal interface, a slight re-oxidation of the metal surface by the $^{18}O_2$ present in the ToF-SIMS analysis chamber is observed because it occurs more rapidly than the time between two sputtering in the dual-beam mode used for depth profiling. The consequence is a low intensity signal of $^{18}O^-$ still observed in the substrate region of the depth profile (Fig. 2b), and a high $^{18}O/(^{18}O + ^{16}O)$ ratio (Fig. 2a) because the $^{16}O^-$ signal is very small.

It has been shown above that during the second step (re-oxidation in $^{18}O_2$), the Cr oxide film mainly grows at the metal/oxide interface, by diffusion of the ^{18}O species via anionic defects. However, the non-normalized ToF-SIMS depth profiles obtained after the second re-oxidation step in $^{18}O_2$ (Fig. 2b) show an in-depth

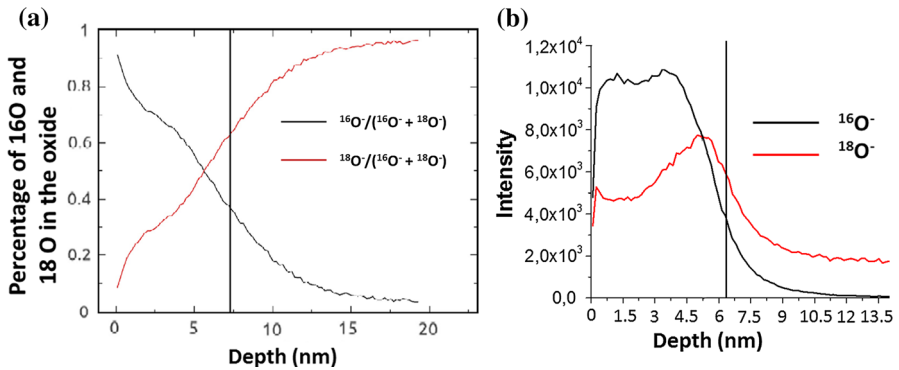


Fig. 2 **a** Intensity ratios $^{16}\text{O}^-/(^{16}\text{O}^- + ^{18}\text{O}^-)$ (black) and $^{18}\text{O}^-/(^{16}\text{O}^- + ^{18}\text{O}^-)$ (red) after 210-min oxidation under $^{16}\text{O}_2$ atmosphere and 1 min under $^{18}\text{O}_2$ and **b** $^{16}\text{O}^-$ and $^{18}\text{O}^-$ ion signals on a ToF-SIMS depth profile after 210-min oxidation under $^{16}\text{O}_2$ atmosphere and 155 min under $^{18}\text{O}_2$. Pressure for both exposures was 6.0×10^{-7} mbar and temperature 300 °C. Vertical line indicates the total thickness of the oxide, defined by the maximum intensity of the Cr_2^- signal (not shown here) (Color figure online)

increase of the $^{18}\text{O}^-$ signal in the Cr oxide layer, even for long re-oxidation times (155 min of re-oxidation in Fig. 2b). This indicates that diffusion is not the only mechanism leading to the presence of ^{18}O species in the Cr oxide film formed during the first oxidation step (oxidation in $^{16}\text{O}_2$). The second mechanism consists in the isotopic exchange between ^{16}O and ^{18}O species that takes place both at the oxide/environment interface (inward isotopic exchange) and also at the interface between the Cr oxide formed during the first oxidation step with $^{16}\text{O}_2$ and the Cr oxide newly formed with ^{18}O species during the re-oxidation step (backward isotopic exchange). A schematic representation of the oxide film, including the possible mechanisms (diffusion and isotopic exchanges) of O species migration in the Cr oxide film, is given in Fig. 3. Thus, both (1) diffusion coefficient of O in the oxide and (2) isotopic exchange coefficient due to the exchange between ^{16}O and ^{18}O in the Cr oxide during the re-oxidation step in $^{18}\text{O}_2$ must be considered. ToF-

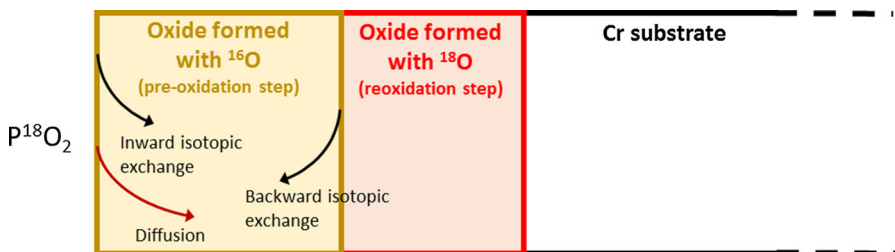


Fig. 3 Schematic representation of the oxide film formed on Cr substrate after pre-oxidation in $^{16}\text{O}_2$ and re-oxidation in $^{18}\text{O}_2$. The mechanisms of O species migration in the Cr oxide film, via diffusion and/or isotopic exchange, are indicated

SIMS depth profiles have already been used to determine apparent diffusion coefficient of Li species in a bulk Si substrate [29] or to study transport mechanisms in an SEI layer [30, 31]. The ToF-SIMS data, reported above on ^{18}O concentration in the oxide film, allow us to calculate both the apparent diffusion coefficient [D , in ($\text{cm}^2 \text{s}^{-1}$)] and the isotopic exchange coefficient [k , in ($\text{at.cm}^{-2} \text{s}^{-1}$)], from the semi-infinite integration of Fick's second diffusion law for one-dimensional diffusion, including isotopic exchange coefficient [32], as follows:

$$\frac{\partial C}{\partial t} = -D \frac{\partial^2 C}{\partial x^2} + k_c \quad (11)$$

where the first term is for diffusion and the second one for isotopic exchange, C is the concentration of ^{18}O in the Cr oxide film at depth x and after oxidation time t . In this model, it is assumed that there is no interaction between diffusion and exchange of ^{18}O species in the Cr oxide film during the re-oxidation step with ^{18}O .

The following boundary conditions are used:

$$\begin{cases} C(x, 0) = 0, & x > 0 \\ C(0, t) = C_0, & t > 0 \\ C(x = M/O, t) = C_{\max}, & t > 0 \end{cases} \quad (12)$$

with C_{\max} , the initial ^{18}O concentration at the metal/oxide interface; C_0 , the initial ^{18}O concentration at the outer interface ($x = 0$). Considering that both ^{18}O diffusion coefficient (D) and isotopic exchange coefficient (k) are independent of x and C , the analytical solution of Eq. 1, 2 gives:

$$\begin{aligned} \frac{C(x, t) - C_{\max}}{C_0 - C_{\max}} = \frac{1}{2} \left\{ \exp - \left(\sqrt{\frac{k}{D}} x \right) \operatorname{erfc} \left(\frac{x}{2\sqrt{Dt}} - \sqrt{kt} \right) \right. \\ \left. + \exp \left(\sqrt{\frac{k}{D}} x \right) \operatorname{erfc} \left(\frac{x}{2\sqrt{Dt}} + \sqrt{kt} \right) \right\} \end{aligned} \quad (13)$$

which is a concentration profile as a function of time $C(x, t)$. Hence, Eq. 13 describes ^{18}O ion accumulation in the Cr oxide with time, that is, changes in concentration profile and concentration gradient with time.

Figure 4 shows the normalized ToF-SIMS profile (I/I_0), which reflects the normalized concentration profile (C/C_0) (since I is proportional to C in a ToF-SIMS experiment) of the $^{18}\text{O}^-$ species after 155 min of re-oxidation in $^{18}\text{O}_2$ and the fit of the data (solid line) using the model presented above. It is observed that, after 155 min of re-oxidation in $^{18}\text{O}_2$, the model fits very well the experimental data, excepted at the surface. This can be explained by a permanent modification of the surface oxide due to the volatilization of the Cr_2O_3 oxide film during the experiment, as previously demonstrated. The O diffusion coefficient and the isotopic exchange coefficient determined in this way are $2 \times 10^{-18} \text{cm}^2 \text{s}^{-1}$ and $2 \times 10^{-11} \text{at.cm}^{-2} \text{s}^{-1}$, respectively. These values are in good agreement with the ones found in the literature for D ($4 \times 10^{-17} \text{cm}^2 \text{s}^{-1}$, extrapolated at 300 °C) [33] and k ($6 \times 10^{-12} \text{at.cm}^{-2} \text{s}^{-1}$ at 400 °C) [32].

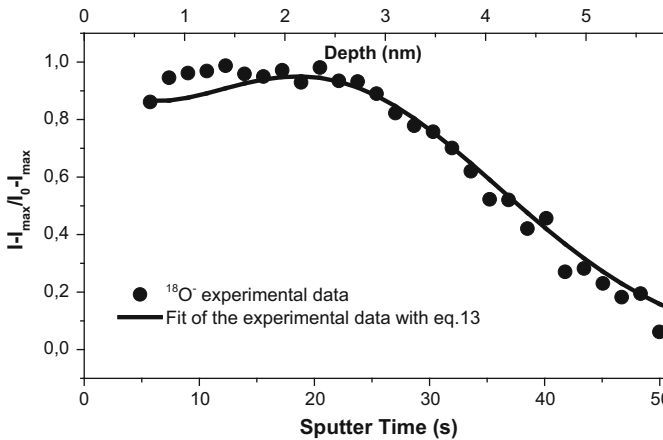


Fig. 4 Normalized I/I_0 ToF-SIMS depth profile of the $^{18}\text{O}^-$ signals after 210 min oxidation under $^{16}\text{O}_2$ atmosphere and 155 min under $^{18}\text{O}_2$. Pressure for both exposures was 6.0×10^{-7} mbar and temperature 300°C . The solid line is the fit of the ToF-SIMS data with Eq. 13 to find both diffusion coefficient and isotopic exchange coefficient of O in the Cr oxide

Conclusions

The oxidation of Cr at 300°C has been investigated in situ by ToF-SIMS for three different O_2 partial pressures. Although it is known that volatilization of Cr_2O_3 occurs at high temperature, it has also been evidenced in this work at 300°C .

Another feature of Cr oxidation reported in this work is that the order of maximum thickness reached by the oxide layers does not correspond to the order of oxygen partial pressure they were exposed to. Exposure to the intermediate pressure ($P_{\text{O}_2} = 6.0 \times 10^{-7}$ mbar) results indeed in the thinnest oxide layer, whereas exposures to the lowest and highest pressures ($P_{\text{O}_2} = 2.0 \times 10^{-7}$ mbar and $P_{\text{O}_2} = 2.0 \times 10^{-6}$ mbar) result in the intermediate and thickest layers, respectively. This feature is the result of a competition between parabolic growth and volatilization occurring at 300°C . This is well fitted by the Tedmon model.

The dependence of the parabolic and volatilization constants, k_p and k_v , to oxygen partial pressure was found to be in $P^{-1/2}$. This dependence indicates that oxygen vacancies are the major defects in the oxide layer and that inward oxygen diffusion is the governing mechanism of oxidation for those low pressures. Two-stage oxidation experiments consisting of a first exposure to $^{16}\text{O}_2$ followed by an exposure to $^{18}\text{O}_2$ isotopic tracer were performed. Depth profiles showed clear evidence of new ^{18}O oxide formation at the metal/oxide interface, providing direct evidence that the oxidation mechanism is governed by inward diffusion of oxygen. From the ToF-SIMS profiles, and using an appropriate model developed in this work, the diffusion coefficient of O species in the oxide film and the isotopic exchange coefficient have been determined. They are $2 \times 10^{-18} \text{ cm}^2 \text{ s}^{-1}$ and $2 \times 10^{-11} \text{ at.cm}^{-2} \text{ s}^{-1}$, respectively.

Acknowledgements Financial supports by EDF R&D and by Région Ile-de-France are acknowledged.

References

1. R. Sachitanand, M. Sattari, J. E. Svensson and J. Froitzheim, *International Journal of Hydrogen Energy* **38**, 15328 (2013).
2. S. P. Jiang and Y. Zhen, *Solid State Ionics* **179**, 1459 (2008).
3. V. A. C. Haanappel, T. Fransen and P. J. Gellings, *High Temperature Materials and Processes* **10**, 91 (1992).
4. E. J. Opila, *Journal of the American Ceramic Society* **86**, 1238 (2003).
5. Y. Chen, T. Tan and H. Chen, *Journal of Nuclear Science and Technology* **45**, 662 (2008).
6. D. J. Young and B. A. Pint, *Oxidation of Metals* **66**, 137 (2006).
7. R. O. Adams, *Journal of Vacuum Science and Technology A* **1**, 12 (1983).
8. J. R. Lince, S. V. Didziulis, D. K. Shuh, T. D. Durbin and J. A. Yarmo, *Surface Science* **277**, 43 (1992).
9. A. P. Gree, C. W. Louw and H. C. Swart, *Corrosion Science* **42**, 1725 (2000).
10. W. T. Geng, *Physical Review B* **68**, 233402 (2003).
11. L. Pramatarova, E. Pecheva, V. Krastev and F. Riesz, *Journal of Materials Science: Materials in Medicine* **18**, 435 (2007).
12. P. Jussila, K. Lahtonen, M. Lampimäki, M. Hirsimäki and M. Valden, *Surface and Interface Analysis* **40**, 1149 (2008).
13. P. Jussila, H. Ali-Löyty, K. Lahtonen, M. Hirsimäki and M. Valden, *Surface Science* **603**, 3005 (2009).
14. A. C. S. Sabioni, A. M. Huntz, J. Philibert, B. Lesage and C. Monty, *Journal of Materials Science* **27**, 4782 (1992).
15. K. P. Lillerud and P. Kofstad, *Journal of the Electrochemical Society* **127**, 2397 (1980).
16. K. P. Lillerud and P. Kofstad, *Oxidation of Metals* **17**, 127 (1982).
17. M.Y. Su, and G. Simkovitch, Technical report of the Applied Research Laboratory of the Pennsylvania State University (1987).
18. C. Wagner, *Journal of the Electrochemical Society* **99**, 369 (1952).
19. N. Cabrera and N. F. Mott, *Reports on Progress in Physics* **12**, 163 (1949).
20. D. D. Eley and P. R. Wilkinson, *Proceedings of the Royal Society of London A* **254**, 327 (1960).
21. F. P. Fehlner and N. F. Mott, *Oxidation of Metals* **2**, 59 (1970).
22. C. S. Tedmon, *Journal of the Electrochemical Society* **113**, 766 (1966).
23. A. Mazenc, A. Galtayries, A. Seyeux, P. Marcus and S. Leclercq, *Surface and Interface Analysis* **45**, 583 (2013).
24. A. Mazenc. Ph.D. thesis, Université Pierre et Marie Curie (2013).
25. P. Kofstad, *Oxidation of Metals* **44**, 3 (1995).
26. J. H. Park, W. E. King and S. J. Rothman, *Journal of the American Ceramic Society* **70**, 880 (1987).
27. A. C. S. Sabioni, E. A. Malheiros, V. Ji, F. Jomard, W. A. de Almeida Macedo and P. Gastelois, *Oxidation of Metals* **81**, 407 (2014).
28. S. C. York, M. W. Abee and D. F. Cox, *Surface Science* **437**, 386 (1999).
29. C. Pereira-Nabais, J. Swiatowska, M. Rosso, F. Ozanam, A. Seyeux, A. Gohier, P. Tran-Van, M. Cassir and P. Marcus, *ACS Applied Materials and Interfaces* **6**, 13023 (2014).
30. P. Lu and S. J. Harris, *Electrochemistry Communications* **13**, 1035 (2011).
31. S. Shi, P. Lu, Z. Liu, Y. Qi, L. G. Hector, H. Li and S. J. Harris, *Journal of the American Chemical Society* **134**, 15476 (2012).
32. G. K. Boreskov, *Advances in Catalysis* **15**, 285 (1965).
33. W. C. Hagel, *Journal of the American Ceramic Society* **48**, 70 (1965).